MICROCALCIFICATION DETECTION BASED ON LOCALIZED TEXTURE COMPARISON

Xin Yuan[1,2] *and Pengcheng Shi*[1]

[1]Medical Image Computing Group, Department of Electrical and Electronic Engineering
Hong Kong University of Science and Technology, Clear Water Bay, Kowloon, Hong Kong
[2]College of Computer Science, Zhejiang University, Hangzhou 310027, China

ABSTRACT

While microcalcifications (MCs) are important early signs of breast cancers, their reliable detection from mammograms has been largely elusive for both radiologists and computer-aided diagnosis (CAD) strategies. Two of the essential components in a CAD system are the detection of the suspicious MC pixels/regions using image processing and analysis techniques, and the training, classification, and recognition of these areas based on pattern recognition methods. In this paper, we present a novel scheme to identify and classify microcalcifications based on localized texture comparison. Relying on a texture removal and repairing (R&R) process of the preselected suspicious areas from their surrounding background tissues, pre- and post- R&R local characteristic features of these areas are extracted and compared. A modified AdaBoost algorithm is then adopted to train the classifier using expert-labelled microcalcifications, followed by a clustering process. Experiments with the mammographic images from the MIAS and DDSM databases have shown very promising results.

1. INTRODUCTION

Microcalcifications are the earliest signs of breast cancers, appearing in mammographic images as small (0.05–1mm in diameter) and bright spots embedded within non-stationary backgrounds [11] (see examples in Fig. 1). Reliable MC detection has been sofar an extremely difficult task because of the projection nature of mammogram, the low image contrast in high tissue density regions [17], the varying shapes of the legions, the blurred margins of the MCs, and the different types of noises caused by the x-ray imaging and digitization processes. Computer-aided detection and diagnosis (CAD) schemes, based on computer vision and pattern recognition strategies, have been developed to improve the detection rate and to reduce the false positives.

Mammogram analysis in general, and MC detection in particular, can be divided into three sequential steps: the enhancement of image features, the localization of suspicious areas, and the training and classification of these areas [7]. Once images are preprocessed, i.e. the breast is segmented from the background, various filtering techniques have been popular in recent studies for the suspicious area localization, including wavelet transforms [14], Gabor filters [4], optimal filters [10], and nonlinear morphological operations [3]. Normally, after locating these suspicious areas, salient image features are extracted for further recognition. Existing training and classifying techniques for MC detection include artificial neural networks [5], support vector machine [8], association rule-based classifier [18], etc.

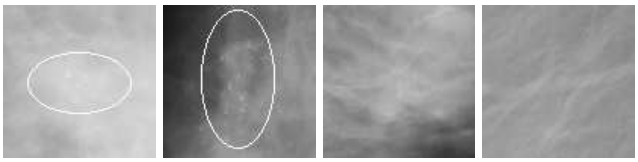

Fig. 1. Mammographic images (cut from the original images): microcalcification legions (left two) and normal tissues (right two).

These existing methods typically compare various image features of the extracted suspicious areas to those of the entire image. However, from the observations that normal tissues far away from the MCs are often of little relevance to the materialistic changes of the MCs, we believe that the comparison between the local characteristic features, when properly extracted, of the suspicious tissues and their *surrounding tissues*, are of particularly great importance for proper MC detection. This motivates us to develop a new approach to make direct texture comparison between a suspicious area and its localized neighborhood through a texture removal and repair process. The resulting features are then trained and classified with a modified AdaBoost algorithm.

2. METHODOLOGY

The overall flow of our MC detection scheme is shown in Fig. 2. In this paper, we focus on the recognition of individual microcalcifications based on localized texture comparison.

2.1. Preprocessing

The goal of the preprocessing is to segment the breast area from image background, to remove certain noises, to mark suspicious MC pixels, and to generate the suspicious MC blobs (see [17]).

Because any mammographic image consists of breast tissues and background area, its image intensity histogram is typically bimodal. It is thus quite easy to select a proper threshold I_{th} to separate the breast tissues from the background by searching the middle point between two modal peaks in the histogram. Further, it has been observed that local image contrast is a suitable measurement for discrimination of the suspicious MC pixels within an image. Since the contrast of microcalcifications in relatively darker area is actually larger than that of brighter area [11, 17], the lower bound of the MC contrast should be a function of the background intensity. We have used the profiles of the multi-orientation

0-7803-8554-3/04/$20.00 ©2004 IEEE.

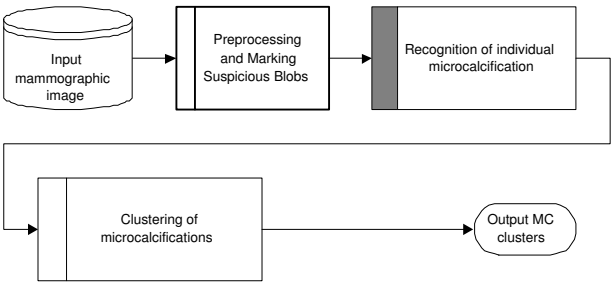

Fig. 2. System flowchart.

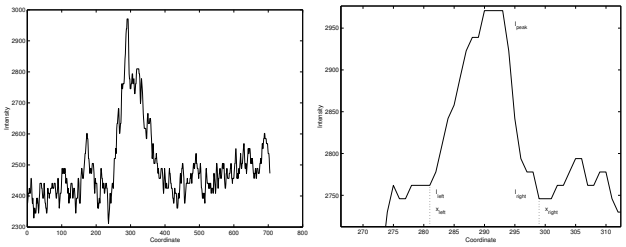

Fig. 3. An example image scanline (left) and corresponding contrast analysis curve (right).

image scanlines (horizontal, vertical, diagonal, and anti-diagonal) to obtain pixel contrast, which is evaluated as the minimum of the two difference values from the peak to the left and right valleys (Fig. 3 shows an example of the scanline and the pixel contrast analysis). In order to obtain the discriminant functions of contrast and image intensity, a training process posed as an optimization problem is needed.

Suspicious MC blobs is generated from the marked suspicious MC pixels using morphological operations. A blob is discarded if its size is larger than an area threshold, $W_m \times W_m$, which is dependent on the image resolution.

2.2. Recognition of Individual Microcalcification

2.2.1. Blob Removal and Repair: Local Texture Inpainting

As mentioned earlier, it is not sufficient to use image features from the suspicious MC blobs alone for classification and recognition, as most existing efforts have done sofar. Rather, the differences between an MC blob and its immediate neighbor are of paramount importance for reliable MC classification and recognition.

Since normal breast tissues exhibits continuous image texture properties, any void of the normal tissue, especially if it is of small size, can be theoretically *recovered*, to certain extent, from its surrounding tissues. Thus, if we remove a suspicious MC blob from the mammogram and use local texture inpainting technique to *repair* the void, and then compare the image textures between the pre- and post-repaired blob, we can get direct measurements on the differences between the blob and its surrounding normal tissues *on the same scale*. If the blob is a microcalcification, it would not be able to be recovered by the surrounding normal tissues, and thus the difference would be substantially different from the case where the blob is of mis-labelled normal tissues.

Because the breast tissues have relatively high local variations, we have experienced difficulties in obtain reasonably good inpainting results using existing inpainting techniques [6, 12], and we have developed a new texture-like inpainting approach based on wavelet diffusion. Since the variation of the mammogram intensity reflects the changes of tissue types and thickness [17], we regard these signals as the linear combination of some basis functions and the texture inpainting now becomes a diffusion process of these basis functions. Since the wavelet theory is suited for the analysis of local scale phenomena [13], we have used wavelet subbands diffusion to implement our texture inpainting process. For computational simplicity, we only use the weighted average of wavelet subbands decomposed from the blob's neighboring blocks to estimate the blob's wavelet subbands, and obtain the *repaired* blob image through inverse wavelet transform.

A wavelet transform is computed with several mother wavelets ψ_k $(1 \le k \le K)$, with K the number of spatial orientations. Denote $\psi_{k,s}(x,y) = \frac{1}{s}\psi_k\left(\frac{x}{s}, \frac{y}{s}\right)$, and select the basis functions $\psi_{k,s}$ as an orthogonal basis, image $I(x,y)$ can be expressed as [13]:

$$I(x,y) \quad = \quad \sum_s \frac{1}{s}\left[\sum_{k=1}^{K} W_{k,s}(x,y) * \psi_{k,s}(x,y)\right] \qquad (1)$$

In our work, we use only one scale to decompose the image, and get four subbands (smoothing, horizontal, vertical, and diagonal), denoted as W_{LL}, W_{HL}, W_{LH}, and W_{HH}, which represent responses of different orientations.

Let I_i, $(1 \le i \le N)$, denote the neighboring subblocks of blob I which is being repaired, and $d(I_i, I)$ denote the distance between I_i and I, we use the following weighted average of subbands to estimate the wavelet subbands of blob I, and use Equation (1) to reconstruct the inpainted blob $I_{inpaint}$:

$$\begin{aligned}
W_{LL}(x,y) &= \frac{1}{C}\sum_{i=1}^{N} e^{-d(I_i,I)} W^i_{LL}(x,y) \\
W_{HL}(x,y) &= \frac{1}{C}\sum_{i=1}^{N} e^{-d(I_i,I)} W^i_{HL}(x,y) \\
W_{LH}(x,y) &= \frac{1}{C}\sum_{i=1}^{N} e^{-d(I_i,I)} W^i_{LH}(x,y) \\
W_{HH}(x,y) &= \frac{1}{C}\sum_{i=1}^{N} e^{-d(I_i,I)} W^i_{HH}(x,y) \\
C &= \sum_{i=1}^{N} e^{-d(I_i,I)}
\end{aligned}$$

The advantage of this inpainting scheme is that, in theory, local structure can be *recovered* after repairing. Visual appearance of the repaired void is actually not important here, because we only care for the blob's texture features before and after the inpainting process. Hence, the appearance continuity between the blob and its background is not necessary achieved. Nevertheless, visually plausible inpainting result is shown in Fig. 4.

2.2.2. Local Characteristic Features

Pre- (I) and post-repairing ($I_{inpaint}$) blob features are defined as following:

- M_s: the post-inpainting mean intensity of the *support domain* of the blob, which includes the blob and its surrounding subblocks I_i;

Fig. 4. Local texture repairing of suspicious blobs: pre-repairing (left), blob removal (middle), and post-inpainting (right).

- S_I: area of the blob;
- N_s: number of suspicious blobs within the support domain of blob I;
- post-inpainting average energies of the detailed subbands of the blob support domain, which reflect the texture information of the support domain:

$$E_{HL} = \frac{1}{M_{HL} \times N_{HL}} \sum_{i=1}^{M_{HL}} \sum_{j=1}^{N_{HL}} |W_{HL}(i,j)|$$

$$E_{LH} = \frac{1}{M_{LH} \times N_{LH}} \sum_{i=1}^{M_{LH}} \sum_{j=1}^{N_{LH}} |W_{LH}(i,j)|$$

$$E_{HH} = \frac{1}{M_{HH} \times N_{HH}} \sum_{i=1}^{M_{HH}} \sum_{j=1}^{N_{HH}} |W_{HH}(i,j)|$$

  where M_{HL}, M_{LH}, and M_{HH} are widths, N_{HL}, N_{LH} and N_{HH} are heights of the wavelet subbands, and W_{HL}, W_{HL} and W_{HL} are the wavelet coefficients;
- ΔM_s: difference between the pre- and post-inpainting mean intensity values of the blob support domain;
- $(\Delta\sigma_s)$: difference between the pre- and post-inpainting intensity standard deviations of the blob support domain;
- ΔV_{max}: difference between the pre- and post-inpainting maximum intensity values of the blob support domain;
- ΔE_{HL}, ΔE_{LH}, and ΔE_{HH}: differences between the pre- and post-inpainting average energies of the detailed subbands of the blob support domain.

2.2.3. Feature Training and Classification

In the training step, we adopt and modify the AdaBoosting algorithm which boosts a series of weak classifiers into a strong classifier [9, 15]. The rationale is that AdaBoosting allows a certain number of false positives after each classification process, thus conceptually better handles the issue of feature overlapping between the normal and microcalcification tissues.

Given l training samples $(\mathbf{x}_1, y_1), (\mathbf{x}_2, y_2), \ldots, (\mathbf{x}_l, y_l)$, $\mathbf{x}_i \in \mathbf{X}$ where $\mathbf{X}$ is a N-dimensional feature space, $y_i \in \mathbf{Y} = \{-1, +1\}$ where $\mathbf{Y}$ are labels for positive and negative samples, and weights C^+ and C^-:

1. Let $t = 1$, initialize:

$$\omega_i^{(1)} = \begin{cases} \frac{C^+}{C^+ + C^-} \cdot \frac{1}{m^+} & \text{if } y_i = +1 \\ \frac{C^-}{C^+ + C^-} \cdot \frac{1}{m^-} & \text{if } y_i = -1 \end{cases}$$
$$i = 1, 2, \ldots, l$$

   where m^+ and m^- are the numbers of positive and negative samples respectively, with $m^+ + m^- = l$.

2. Train a weak classifier $h_t(\mathbf{x}) = sign(x_t - h_t)$ using distribution $\omega_i^{(t)}$, i.e. minimize

$$R_{emp}(\mathbf{x}) = -\sum_{i=1}^{l} \omega_i^{(t)} y_i h_t(\mathbf{x}_i)$$

   where x_t is an element of the feature vector, and h_t is a threshold value of the element pre-decided for this step.

3. Calculate the training error:

$$\epsilon_t = \sum_{h_t(\mathbf{x}_i) \neq y_i} \omega_i^{(t)}$$

4. Choose

$$\alpha_t = \frac{1}{2} \ln \frac{1 - \epsilon_t}{\epsilon_t}$$

5. Update:

$$\omega_i^{t+1} = \omega_i^t e^{[-\alpha_t y_i h_t(\mathbf{x}_i)]},\ i = 1, 2, \ldots, l$$

6. Normalize:

$$\omega_i^{t+1} = \frac{\omega_i^{t+1}}{\sum_{i=1}^{l} \omega_i^{t+1}},\ i = 1, 2, \ldots, l$$

7. Let $t = t + 1$, if $t \leq N$, goto step 2; otherwise, stop.

Hence, the final decision function becomes:

$$H(\mathbf{x}) = sign\left[\sum_{t=1}^{N} \alpha_t h_t(\mathbf{x})\right] \quad (2)$$

2.3. Clustering of Microcalcifications

Clustered microcalcifications are one of the earliest signs of potential cancerous changes in breast tissues. A cluster is typically defined to have at least 2 or 3 MCs within a $1cm^2$ region [10]. We have used a simple clustering method to generate the MC clusters: 1) add a blob to an existing cluster if the distance from the blob to the center of cluster is less than D_I, otherwise create a new cluster and add this blob to it; 2) if the center distance between two clusters is less than D_c, they are merged; and 3) a cluster is removed if the number of blobs in it is less than N_c (a threshold defined by radiologists). The other two thresholding parameters in the process, D_I and D_c, are dependent on the resolution of the mammogram.

3. EXPERIMENTAL RESULTS

Our method has been evaluated using two well known, publicly available mammographic image databases: the Mammographic Image Analysis Society (MIAS) database [2] and the Digital Database for Screening Mammography (DDSM) [1].

The MIAS database consists of 322 images, digitized in 200 micron per pixel resolution, 1024×1024 in size, and 8-bit in depth. There are 24 images containing 29 microcalcification clusters in the data set. We have randomly selected 11 images containing 14

Study	images used	TP rate (%)	FP per image
Gulsrud [10]	43	100	2.3
Zaïane [18]	322	80.33	near 0
Ours	322	93.3	4.8

Table 1. MC detection results using the MIAS database.

MC clusters as the training set for our experiment, and remaining 311 images have been used the testing set.

In the training set, after preprocessing with $W_m = 5$, we obtained suspicious 471 blobs in total. We then used the 4^{th}-order Deubechies wavelets to decompose the subblocks for one level in the texture-inpainting step. The size of the support domain was set to 10×10. Fig. 4 illustrates texture-inpainting results for image mdb236, where obviously the appearance of the repaired void is very similar to the background normal tissues, as we hoped. Classifier was trained with $C^+ = 0.9$ and $C^- = 0.1$, and clustering process was performed with $D_I = 50$, $D_c = 25$, and $N_c = 3$. 311 test images went through the same procedures, and we achieved the detection results of 93.3% true positive rate with 4.8 false positives per image. While Table 1 lists our results as well as other two studies using the MIAS database, it is difficult to make completely meaningful and direct comparison on the effectiveness of various methods because different mammograms from the MIAS database were used for training and testing.

Recognized as one of the most difficult databases, there have been few algorithms trained and tested on the DDSM dataset. In our experiment, as suggested by the DDSM authors for fair comparison [1], we used the BCRP_CALC_0 images as the training set and the BCRP_CALC_1 images as the test set. Each set contains 50 cases and each case consists of four images (CC-view and MLO-view for the left and right breasts). Spatial resolution for these mammograms is 43.5 microns, and each mammogram has an overlay file which describes the boundary coordinates of ground truth clustered microcalcifications in the form of chain coding. We selected 99 calcifications-containing regions-of-interests (ROIs) from the training set, which were used to train the classifier for the marked suspicious pixels with $W_m = 23$. After a region growing process, we obtained 341103 blobs in total. In the feature extraction step, the size of support domain was set to 34×34. Finally, a dynamic clustering algorithm was performed to obtain clustered microcalcifications using $D_I = 230$, $D_c = 115$, and $N_c = 3$. All 50 cases in the test set were processed under the same procedures and parameters. Overall, we achieve the detection results with 90.1% true positive rate and 15.4 false positives per image. Compared to an earlier algorithm on the same database which has achieved 69.5% true positive rate and 2.11 false positives per image [16], our method has better true positive rate. However, the false positive rate is too high for practical purposes and has become our current research focus, including the possibilities of introducing image and feature space normalization.

This work is supported in part by Hong Kong Research Grant Council through HKUST-DAG02/03.EG45.

4. REFERENCES

[1] Digital database for screening mammography. http://marathon.csee.usf.edu/Mammography/Database.html.

[2] Digital mammography database of the mammographic image analysis society. http://www.wiau.man.ac.uk/services/MIAS/MIASweb.html.

[3] D. Betal. Extraction of microcalcifications from digital mammograms using mathematical morphology. In *IEE Colloquium on Morphological and Nonlinear Image Processing Techniques*, 9, pages 1–3, 1993.

[4] T. Bhangale, U.B. Desai, and U. Sharma. An unsupervised scheme for detection of microcalcifications on mammograms. In *IEEE International Conference on Image Processing*, volume 1, pages 184–187, 2000.

[5] H.P. Chan, S.C.B. Lo, B. Sahiner, K.L. Lam, and M.A. Helvie. Computer-aided detection of mammographic microcalcifications: Pattern recognition with an artificial neural network. *Medical Physics*, 22(10):1555–1567, 1995.

[6] T.F. Chan and J. Shen. Inpainting based on nonlinear transport and diffusion. In *Inverse problems, image analysis, and medical imaging*, volume 313, pages 53–65. 2002.

[7] Y. Chitre, A.P. Dhawan, and M. MoskoWitz. Artificial neural network based classification of mammographic microcalcifications using image structure features. In *State of The Art in Digital Mammographic Image Analysis*, pages 167–197. World Scientific, 1994.

[8] I. El-Naqa, Y. Yang, M.N. Wernick, N.P. Galatsanos, and R. Nishikawa. A support vector machine approach for detetcion of microcalcifications in mammograms. In *IEEE International Conference on Image Processing*, pages 201–204, 2002.

[9] Y. Freund and R.E. Schapire. Experiments with a new boosting algorithm. In *International Conference on Machine Learning*, pages 148–156, 1996.

[10] T.O. Gulsrud, J.H. Husøy, and H. Stavanger. Optimal filter for detection of clustered microcalcifications. In *International Conference on Pattern Recognition*, volume 1, pages 508–511, 2000.

[11] R. Highnam and M. Brady. *Mammographic Image Analysis*. Kluwer Academic Publishers, 1999.

[12] J. Jia and C.K. Tang. Image repairing: robust image synthesis by adaptive nd tensor voting. In *IEEE Computer Vision and Pattern Recognition*, volume 1, pages 643–650, 2003.

[13] S. Mallat. *A Wavelet Tour of Signal Processing*. Academic Press, San Diego CA, 1998.

[14] R.N. Strickland and H.I. Hahn. Wavelet transforms for detecting microcalcifications in mammograms. *IEEE Transactions on Medical Imaging*, 15(2):218–229, 1996.

[15] V.N. Vapnik. *The Nature of Statistical Learning Theory*. Springer, New York, 2000.

[16] N.C. Yarlagadda, K.W. Bowyer, and R. Li. Baseline comparison of microcalcification detection algorithms. In *International Workshop on Digital Mammography*, pages 414–420, 2000.

[17] X. Yuan and P.C. Shi. The physical nature of mammographic image processing. Technical report, Hong Kong University of Science and Technology, 2003.

[18] O.R. Zaïane, M.-L. Antonie, and A. Coman. Mammography classification by an association rule-based classifier. In *ACM SIGKDD: International Workshop on Multimedia Data Mining*, pages 62–69, 2002.